Biomaterials Science

ROYAL SOCIETY OF CHEMISTRY

PAPER

View Article Online
View Journal | View Issue

Cite this: *Biomater. Sci.*, 2024, **12**, 1477

Nitric oxide-scavenging hyaluronic acid nanoparticles for osteoarthritis treatment†

Yunyoung Nah,[a] Sivasangu Sobha,[b] Gurusamy Saravanakumar,[b] Byung-Yoon Kang,[b] Joo-Byoung Yoon[b] and Won Jong Kim *[a,b,c]

Osteoarthritis (OA) is a degenerative arthritis disease marked by inflammation, pain, and cartilage deterioration. Elevated nitric oxide (NO) levels play a pivotal role in mediating OA-related inflammation and are found in abundance within OA joints. This study introduces a NO-scavenging hyaluronic acid conjugate (HA–NSc) bearing both lubrication and anti-inflammatory properties for the treatment of osteoarthritis. For this, a derivative of *o*-phenylenediamine (*o*-PD) with good NO-scavenging capability (NSc) is designed, synthesized and chemically conjugated to HA. Owing to the amphiphilicity, this as-synthesized HA-NSc conjugate formed self-assembled nanoparticles (HA–NSc NPs) under aqueous conditions. When treated with activated murine macrophage RAW 264.7 cells that produce high levels of NO, these nanoparticles effectively reduced intracellular NO concentrations and inflammatory cytokines. In an OA animal model, the HA–NSc NPs significantly alleviated pain and diminished the cartilage damage due to the combined lubricating property of HA and NO-scavenging ability of NSc. Overall, the results from the study suggest HA–NSc NPs as a dual-action therapeutic agent for the treatment of OA by alleviating pain, inflammation, and joint damage, and also positioning the HA–NSc NPs as a promising candidate for innovative treatment of OA.

Received 25th November 2023,
Accepted 17th January 2024

DOI: 10.1039/d3bm01918g

rsc.li/biomaterials-science

1. Introduction

Osteoarthritis (OA) is a debilitating disease characterized by degenerative changes in joint cartilage, leading to chronic inflammation, and pain.[1–3] While the exact pathophysiological mechanisms of OA are not fully understood, multiple biological factors disrupt cartilage homeostasis, resulting in the impaired ability of joints to withstand mechanical forces.[4–6] Consequently, this leads to reduced mobility and a subsequent decrease in the quality of life, and a substantial economic burden due to ongoing costs of treatment.[7] OA, a prevalent age-related degenerative disease, affected over 595 million individuals globally in 2020. Generally, it exhibits a higher prevalence among women as compared to men.[8] Current therapeutic approaches primarily focus on managing pain and controlling inflammation.[9–11] Common medications include non-steroidal anti-inflammatory drugs (NSAIDs) and selective cyclo-oxygenase-2 (COX-2) inhibitors. Alternative options, such as biological agents,[9] intra-articular steroid injections, and injections of lubricants like hyaluronic acid (HA),[12] are available. In severe cases, joint replacement surgery may be necessary.[13] However, these treatments have limitations. Prolonged pharmaceutical treatments can lead to adverse side effects and provide only temporary relief.[14–16] Joint replacement surgeries, while often effective, sometimes require revisions,[17] and involve risks such as dislocation and infection at the surgical site.[18] Therefore, there is a pressing need for innovative, low-risk therapeutic strategies that address the underlying fundamental aspects of OA.

Our study focuses on nitric oxide (NO), a gaseous radical molecule synthesized by nitric oxide synthases (NOSs). NO serves a multitude of crucial functions, including acting as a vasodilator, signaling molecule, and defense mechanisms.[19,20] However, in inflammatory diseases such as OA,[21–23] rheumatoid arthritis (RA),[24] and inflammatory bowel disease (IBD),[25] NO becomes overexpressed and plays a pivotal role in mediating inflammation.[26] In OA, overexpressed NO levels in physically stressed joints[27] and inflammation contributes to the disease's progression through several key mechanisms.[28,29] First, elevated levels of NO induce apoptosis in joint cells, including osteoblasts, osteoclasts, and chondrocytes.[30,31] Second, it sustains signaling pathways such as nuclear factor kappa B (NF-κB), leading to a rise in inflammatory cytokines,

[a]*Department of Chemistry, POSTECH-CATHOLIC Biomedical Engineering Institute, POSTECH, Pohang 37673, South Korea. E-mail: wjkim@postech.ac.kr*
[b]*OmniaMed Co., Ltd, Pohang 37666, Republic of Korea*
[c]*School of Interdisciplinary Bioscience and Bioengineering, Pohang University of Science and Technology (POSTECH), Pohang 37673, South Korea*

† Electronic supplementary information (ESI) available. See DOI: https://doi.org/10.1039/d3bm01918g

such as TNF-α, IL-6, and IL-1β.[32,33] Third, NO influences cartilage degradation by upregulating matrix metalloproteinases (MMPs), like MMP-1, 9, and 13.[34,35] Additionally, NO has been reported to diminish the synthesis of proteoglycan and collagen, contributing to structural changes in cartilage, such as osteophyte growth and meniscal injuries driven by inflammatory factors associated with NO.[28] Therefore, the scavenging of overexpressed NO in OA-affected joints presents a novel and promising approach to the treatment of OA.

Based on previous studies conducted in our laboratory, *o*-phenylenediamine (*o*-PD) derivatives have demonstrated their great promise as effective NO scavengers.[36–39] These *o*-PD derivatives can irreversibly scavenge NO, with their reactivity being enhanced by different functional group substitutions. Moreover, they can be conjugated to polymers without losing their scavenging abilities through specific chemical modifications.[40] In this study, we introduce N^1-(4-aminobutyl)-5-methylbenzene-1,2-diamine (NSc) as a novel NO scavenger with an aminobutyl group for facile polymer conjugation. Hyaluronic acid (HA), an essential component in healthy joints, was selected as the polymer for the NSc conjugation. HA plays vital roles in joints such as hydration and lubrication,[41,42] and is clinically prescribed for OA patients due to its ability to reduce joint friction, protect joint surfaces, and provide pain relief.[12,43] Its biocompatibility and potential for chemical modification have made HA the focus of extensive research in drug delivery systems.[44–46] The objective of this study was to develop HA–NSc conjugate for intra-articular (i.a.) injection into OA joints, with the vision of integrating the following dual functionality for the OA treatment: the lubricating property of HA to alleviate pain and NO-scavenging ability of NSc to reduce the inflammation and cartilage degradation. The as-synthesized NSc was conjugated to HA *via* EDC/HOBt amide coupling reaction, resulting in the synthesis of the HA–NSc conjugate. Notably, this HA–NSc conjugate enable them to self-assemble into nanoparticles (HA–NSc NPs) due to their amphiphilic properties (Scheme 1A). We anticipate that these nanoparticles could extend their retention time within the OA joints by mitigating the HA degradation through scavenging NO *via* NSc moieties, compared to the free HA polymer.[16,47,48] Further, this NO-scavenging ability of the nanoparticles can effectively reduce the levels of pro-inflammatory cytokines at the cellular level. The therapeutic potential of HA–NSc NPs for the treatment of OA was demonstrated by i.a. injection into OA-induced rat as an *in vivo* model (Scheme 1B).

2. Materials and methods

2.1. Materials

Anhydrous dimethyl sulfoxide (DMSO, 99.8%), 4-chloro-3-nitrotoluene (98%), anhydrous tetrahydrofuran (THF ≥ 99.9%), 1-hydroxybenzotriazole hydrate (HOBt ≥ 97.0%), *N*-(3-dimethyaminopropyl)-*N*′-ethylcarbodiimide hydrochloride (EDC ≥ 99.0%), hydrogen chloride solution 4.0 M in dioxane, palladium on carbon (Pd/C, 10 wt%), Amberlyst® A21 free

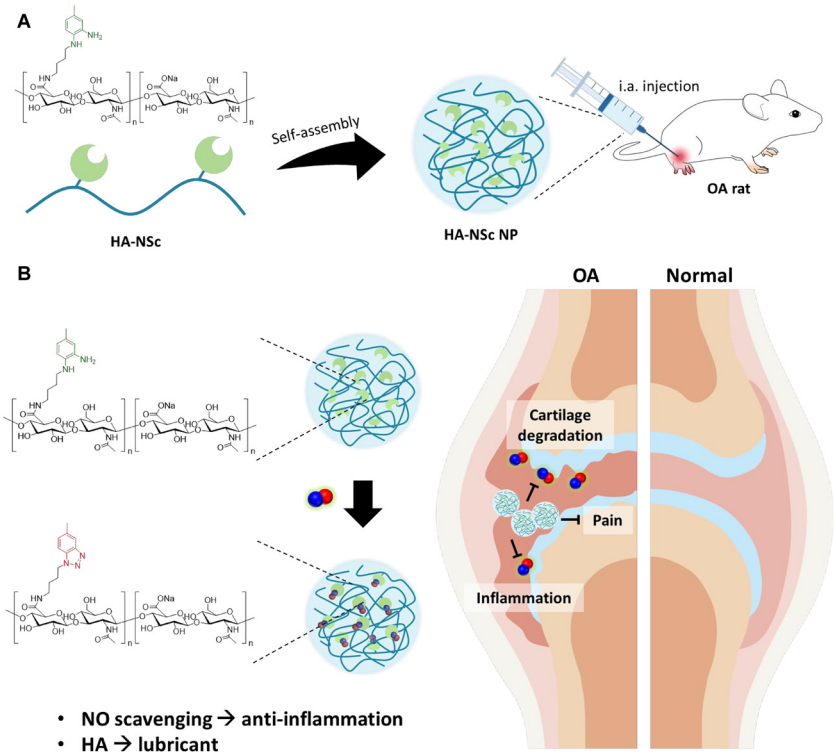

Scheme 1 (A) Self-assembled HA–NSc NPs for OA treatment. (B) Schematic illustration of therapeutic effects of HA–NSc NPs for OA treatment. HA–NSc NPs have dual therapeutic functions; an anti-inflammatory effect through NO scavenging a lubricant derived from HA.

base, Griess reagent (modified), *S*-nitroso-*N*-acetyl-DL-penicillamine (SNAP), 4,5-diaminofluorescein (DAF-2), Thiazolyl Blue Tetrazolium Bromide (MTT), lipopolysaccharides from *Escherichia coli* O111:B4 (LPS), monosodium iodoacetate (MIA), and celecoxib were purchased from Sigma Aldrich (St Louis, MO, USA). *N*-Boc-1,4-butanediamine(≥98.0%) was obtained from TCI chemicals (Tokyo, Japan). Hyaluronic acid (HA, MW = 100 kDa) was purchased from Lifecore Biomedical (Mn, USA). Anhydrous sodium sulfate (Na_2SO_4, 99.0%), 1,4-dioxane (99.5%), methanol (≥99.8%), and Celite® 545 were purchased from Samchun Chemicals Co., (Korea). Fetal bovine serum (FBS), penicillin–streptomycin (P/S), and Dulbecco's Modified Eagles' Medium (DMEM) were purchased from Capricorn Scientific (Germany). DAF-FM diacetate was purchased from Thermo Fisher Scientific.

2.2. Instrumentation

The spectra of ^{1}H nuclear magnetic resonance (^{1}H NMR) were recorded using a Bruker Avance 500 FT-NMR (Avance III 500, Bruker, Germany) with dimethyl sulfoxide (DMSO-d_6) or deuterium oxide (D_2O) as a solvent. Electrospray ionization (ESI) mass analysis was performed using a Thermo Scientific LTQ Velos dual ion trap mass spectrometer equipped with normal ESI source in the positive ion model. Gel permeation chromatography (GPC) measurements were carried out at 40 °C on a hydrophilic GPC LC-20AD system (Shimadzu, Kyoto, Japan) equipped with Shodex OHpack SB-804 HQ and OHpack SB-806M HQ columns. 0.1 M NaCl water was used as an eluent at a flow rate of 1.0 mL min^{-1}. All samples were dissolved in the same eluent solution, and samples were injected after filtration (pore size: 0.2 μm). The ultraviolet-visible (UV-Vis) absorption spectra were recorded by UV-1900i UV-Vis spectrophotometer (Shimadzu, Kyoto, Japan). Sonication was performed using a Sonifier SFX550 equipped with a 1/8″ tapered microtip (Branson, Danbury, USA). The TEM images of nanoparticles were obtained using a BIO TEM JEM-1011 (JEIL Ltd, Tokyo, Japan). The hydrodynamic size distributions of the nanoparticles were measured by a Zetasizer Nano S90 system (Malvern Instruments, Worcestershire, UK). The Griess assay, DAF-2 assay, MTT assay, and ELISA analyses were made on a SpectraMax® i3 microplate reader (Molecular Devices, CA, USA). The fluorescence images were obtained using a Nikon Eclipse Ti-E microscope (Nikon, Tokyo, Japan).

2.3. Synthesis of N^1-(4-aminobutyl)-5-methyl benzene-1,2-diamine (NSc)

The synthesis of NSc was performed in three steps, as shown in Fig. 1A. The products at each step were confirmed by ^{1}H NMR and ESI-MS analysis.

2.3.1. *tert*-Butyl (4-((5-methyl-2-nitrophenyl)amino)butyl) carbamate (compound 2). To a solution of 4-chloro-3-nitrotoluene (6.000 g, 35.086 mmol) in anhydrous DMSO (20 mL), *N*-Boc-1,4-butanediamine (9.908 g, 52.629 mmol) was added. The mixture was stirred at 60 °C overnight. After confirming the completion of the reaction by TLC, the reaction mixture was diluted with distilled water and extracted with dichloromethane. The organic layer was dried with Na_2SO_4 and concentrated *via* rotary evaporation. The final compound **2** was obtained through column chromatography (CH_2Cl_2/MeOH) purification (yield: 4.86 g, 42.9%). ^{1}H NMR (500 MHz, DMSO-d_6) δ 8.04 (s, 1H), 7.87 (d, J = 1.0 Hz, 1H), 7.39 (dd, J = 8.8, 1.9 Hz, 1H), 7.00 (d, J = 8.8 Hz, 1H), 6.85 (s, 1H), 3.34 (s, 4H), 2.95

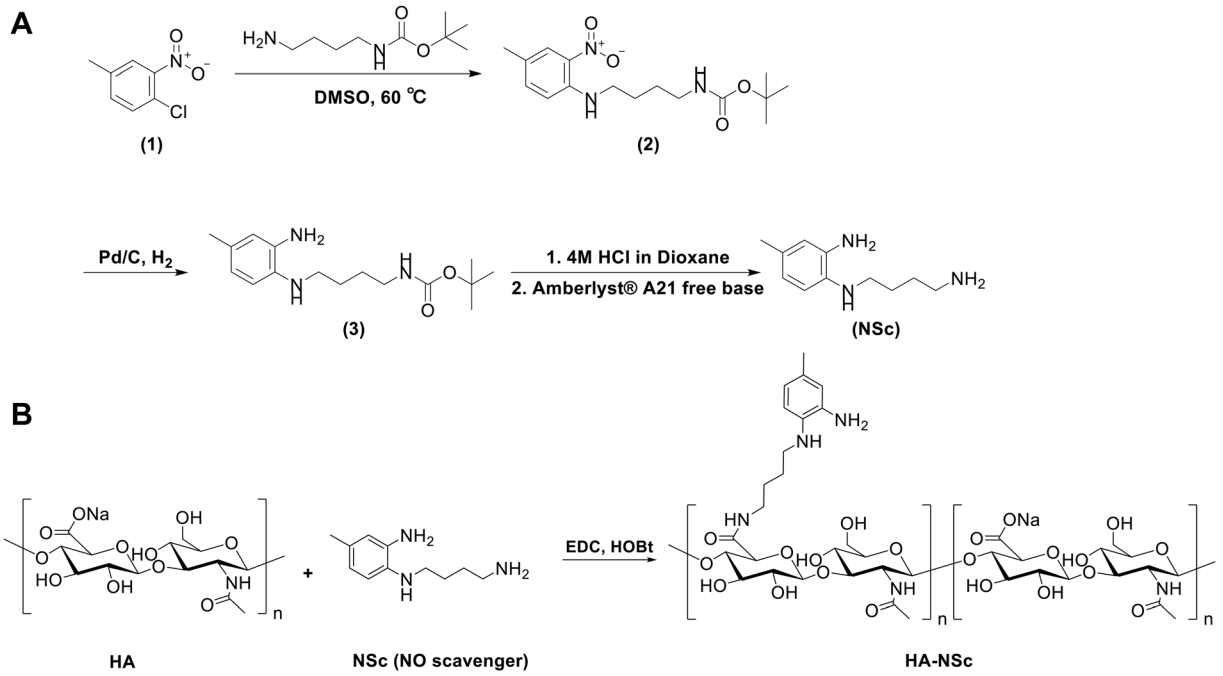

Fig. 1 (A) Synthesis of N^1-(4-aminobutyl)-5-methylbenzene-1,2-diamine (NSc). (B) Synthesis of HA–NSc conjugate.

(d, J = 6.2 Hz, 2H), 2.23 (s, 3H), 1.59 (s, 2H), 1.46 (s, 2H), 1.37 (s, 9H). MS (ESI) m/z $(M + H)^+$: 324.08.

2.3.2. *tert*-Butyl (4-((2-amino-5-methylphenyl)amino)butyl) carbamate (compound 3). To a solution of compound **2** (2.8 g, 8.658 mmol) in anhydrous THF (20 mL), Pd/C (0.280 g) was added. After purging with N_2, the reaction was conducted under a hydrogen atmosphere (assisted by a hydrogen balloon) at room temperature for 24 h. Upon confirmation of the reaction's completion by TLC, the reaction mixture was filtered through a Celite filter. The solvent was removed using the rotary evaporation, and the crude product was purified by column chromatography (CH_2Cl_2/MeOH) to afford the compound **3** (yield: 2.388 g, 94%). ^{1}H NMR (500 MHz, DMSO-d_6) δ 6.82 (s, 2H), 6.29 (s, 3H), 4.42 (s, 4H), 4.12 (t, J = 5.5 Hz, 1H), 3.34 (s, 3H), 2.95 (d, J = 6.1 Hz, 8H), 2.08 (s, 3H), 1.51 (dd, J = 26.6, 6.9 Hz, 4H), 1.38 (s, 9H). MS (ESI) m/z $(M + H)^+$: 294.25.

2.3.3. NO scavenger (NSc). Compound **3** (1.058 g, 3.606 mmol) was dissolved in dioxane (10 mL), followed by the addition of 9 mL of 4 M HCl in dioxane. The reaction mixture was stirred at room temperature, and the reaction completion was verified by TLC. After the reaction, the solvent was removed under reduced pressure to obtain NSc HCl salt. The Nsc HCl salt was desalted by treatment with Amberlyst A21 free base. ^{1}H NMR (500 MHz, DMSO) δ 7.88 (brs, 2H), 6.37 (d, J = 1.1 Hz, 1H), 6.31 (m, 3H), 4.48 (s, 2H), 2.99 (t, J = 6.4 Hz, 2H), 2.81 (t, J = 7.2 Hz, 2H), 2.08 (s, 3H), 1.77–1.50 (m, 4H). MS (ESI) m/z $(M + H)^+$: 194.16.

2.4. Synthesis of HA–NSc conjugate

HA (600 mg) was dissolved in distilled water at a concentration of 5 mg mL^{-1}. Then, EDC (323 mg) and HOBt (228 mg), dissolved in a 1 : 1 mixture of distilled water and DMSO (5 mL), were added to the HA solution under stirring. After adding NSc (325 mg) dissolved in 10 mL of DMSO, the pH of the reaction mixture was adjusted to 6.8. Then the reaction was carried out at room temperature under dark condition for 24 h. The resulting mixture was dialyzed against distilled water for 3 days using a dialysis membrane tube (MW cutoff 3.5 kDa) and lyophilized. The chemical structure of the HA-NSc conjugate was confirmed using ^{1}H NMR (DMSO-d_6/D_2O). The degree of substitution (DS) of NSc, defined as the number of NSc molecules chemically conjugated to 100 repeating units of HA, was calculated from the ^{1}H NMR spectrum was found to be 43. The purification and synthesis of HA–NSc was also confirmed by hydrophilic GPC. The UV-Vis absorption was measured to confirm whether NSc was conjugated to HA.

2.5. Preparation of HA–NSc nanoparticles (HA–NSc NPs)

HA–NSc has the capability to form nanoparticles in aqueous conditions due to its amphiphilic nature. To prepare HA–NSc NPs, the HA–NSc conjugate was suspended in DPBS (pH 7.4) and briefly sonicated for 1 min. After filtration (pore size: 0.45 μm), the hydrodynamic size of HA–NSc NPs was measured using DLS. The morphology of the nanoparticles was observed by TEM using a carbon-coated grid where the nanoparticles were stained with 1% uranyl acetate.

2.6. Stability of HA and HA–NSc conjugate after incubation with NO

The stability of HA polymer and HA–NSc polymer conjugate under high concentrations of NO was analyzed using GPC. In this experiment, SNAP was chosen as the source of NO due to its extended NO release profile resulting from its prolonged half-life.[49] Both HA and HA–NSc conjugate in distilled water at a concentration of 3 mg mL^{-1} were incubated with an equivalent volume of SNAP solution (0, 2, 20, 200 μM) for 24 h at room temperature. Subsequently, the samples were freeze-dried and analyzed using hydrophilic GPC to confirm the possible fragmentation of the polymers.

2.7. Confirmation of NO responsiveness of NSc and HA–NSc

To investigate the effect of NO on the size and morphology of HA–NSc NPs, the nanoparticles were dispersed in distilled water and incubated with NO for 24 h at room temperature. Thereafter, changes in the size and morphology of the nanoparticles were assessed through DLS and TEM imaging, respectively.

The chemical changes of NSc and HA–NSc conjugate after reaction with NO were studied by UV-Vis spectroscopy and ^{1}H NMR spectroscopy. For this, each NSc and HA–NSc conjugate in distilled water at a concentration of 3 mg mL^{-1} was incubated with an equivalent volume of a saturated 100 μM NO solution for 24 h at room temperature. Then, a portion of the samples was taken and the increase in peak intensity within the 280–300 nm range was assessed using UV-Vis spectroscopy. The remaining samples were lyophilized and analyzed using ^{1}H NMR.

2.8. Evaluation of NO scavenging ability of NSc and HA–NSc NPs

The NO scavenging abilities of NSc and HA–NSc NPs were evaluated through Griess assay and DAF-2 assay, following the methods described in previous reports.[38,50] For theses assays, *N*-diazeniumdiolates-incorporated pyrrolidine (PyNO) was employed as the source of NO, and its synthesis was guided by a previous publication.[36] Briefly, pyrrolidine (1.64 mL) was dissolved in a mixture of MeOH (15 mL) and diethyl ether (5 mL). A 30 wt% NaOMe solution (3.9 mL) was added to this mixture, and the reaction was conducted in a high-pressure NO reactor chamber. Following multiple argon purges, the chamber was pressurized with NO gas at 90 psi for 2 days. The PyNO was precipitated by adding cold diethyl ether, filtered, dried in a vacuum oven, and stored at −20 °C and protected from light.

2.8.1. Griess assay. Stock solutions of the samples NSc (4 mM), HA–NSc NPs (37.2 mM, 4 mM of NSc residue), HA (37.2 mM) and physical mixture of HA (37.2 mM) and NSc (4 mM) were prepared in DPBS. After serial dilution of each sample stock solution in a 96-well plate (n = 5), 50 μL of 100 μM PyNO solution was added in each well, and incubated at room temperature for 1 h. Subsequently, 100 μL of Griess reagent was treated in each well, followed by a 15 min incubation in dark conditions. Absorbance was measured at

546 nm, and data was processed by subtracting the background value.

2.8.2. DAF-2 assay. Various stock solutions, including NSc (5 mM), HA–NSc NPs (46.5 mM, 5 mM NSc residue), HA (46.5 mM) and physical mixture of HA (46.5 mM) and NSc (5 mM) were prepared. Additionally, 0.5 mM PyNO stock and 5 mM DAF-2 stock were prepared. In a clean ep-tube, 1 μL of sample stock, 10 μL of DAF-2 stock, and 479 μL of DPBS was added. A control group with only DAF-2 was prepared by using 1 μL DMSO, 10 μL of DAF-2 stock, and 479 μL of DPBS. The background sample was composed of 10 μL of DAF-2 stock and 490 μL of DPBS. Finally, after adding 10 μL of PyNO stock to the sample group, incubation was carried out in the dark for 30 min. Subsequently, 100 μL of each sample was transferred to a 96-well plate (n = 5), and fluorescence was measured (Ex = 495 nm, Em = 520 nm). The relative fluorescence of (DAF-2 only group − background) was set to 100%, and the relative fluorescence of sample was calculated using the formula: (FL value of sample group − FL value of background)/(FL value of DAF-2 only group − FL value of background).

2.9. Cells

The RAW 264.7 cell line was acquired from the Korean Cell Line Bank. These cells were cultured using DMEM medium supplemented with 10% FBS and 1% P/S. The cells were cultured and maintained in a humidified atmosphere with CO_2 at a temperature of 37 °C.

2.10. Cell cytotoxicity test

RAW 264.7 cells were seeded into a 96-well plate with a density of 1×10^4 cells per well. Following an overnight incubation, the culture medium was replaced with fresh medium containing varying concentrations of samples (ranging from 0 to 2 mM of NSc or 0 to 18.6 μM HA and HS–NSc) including HA, NSc, HA + NSc mixture, and HA–NSc (n = 5), with or without the presence of LPS (5 μg mL^{-1}). At this point, the concentration of each sample was determined based on the NSc concentration, where HA–NSc was prepared at the same concentration as the NSc residue, and HA was prepared at the same concentration of HA–NSc. After 48 h incubation, the medium containing the samples was removed. Subsequently, 0.5 mg mL^{-1} of MTT in fresh medium was added to each well. After an additional 4 h incubation, the supernatant was carefully removed, and the purple formazan crystals were dissolved by adding 200 μL of DMSO. The absorbance was measured at a wavelength of 570 nm.

2.11. Confirmation of *in vitro* anti-inflammatory effect

A density of 2×10^5 RAW 264.7 cells were seeded into a 12-well plate, and incubated overnight. Then the culture medium was removed, and LPS (5 μg mL^{-1}) and the samples (PBS, 50 μM of NSc, 0.465 μM of HA–NSc NP and HA, HA + NSc mixture, n = 4) containing medium were added to each well. After 24 h incubation, the supernatant was transferred to ep-tube and centrifuged at 2000 rpm for 15 min to get rid of cellular debris. To evaluate the extracellular NO levels, Griess assay was employed. In brief, 100 μL of supernatant was transferred to a 96-well plate, and then 100 μL of Griess reagent was added to each well. After 15 min incubation, the absorbance was measured at 546 nm. Inflammatory cytokines, including TNF-α and IL-6, were quantified using specific ELISA kits (Koma, Korea). The cell supernatants were stored in deep freezer.

2.12. Intracellular imaging of NO by fluorescence microscopy

For the imaging of intracellular NO, a density of 2×10^5 RAW 264.7 cells were seeded into a 6-well plate and allowed to incubate overnight. The medium was exchanged with either fresh medium or medium containing LPS (5 μg mL^{-1}) and the samples (PBS, HA, NSc, HA + NSc mixture HA–NSc NP). The final concentrations of samples were as follows: 100 μM of NSc, 0.93 μM of HA–NSc NP (equivalent to 100 μM of NSc residue) and HA. After 24 h incubation, the cells were washed with cold DPBS. Then the cells were treated with DAF-FM DA (5 μM) and Hoechst 33342 (10 μM), and stained for 30 min in the dark. Following two additional washed with cold DPBS, the cells were incubated with 10% neutral buffered formalin (NBF) for 10 min in the dark. After a final wash with cold DPBS, fluorescence images were recorded.

2.13. Animal

Our study has been authorized by the IACUC (Institutional Animal Care and Use Committee) to ensure the ethical and scientific treatment of laboratory animals. The research has received approval in accordance with the guidelines established by the Animal Experiment Ethics Committee of the Catholic University of Korea and was conducted within the framework of the approved research protocol (CUMC-2022-0024-01).

2.14. *In vivo* therapeutic effect of HA–NSc in OA model

Prior to inducing the diseases (Day 0), baseline measurements of nociceptive threshold and weight bearing were taken. WISTAR rats (male) were randomly divided into 5 groups (Sham, OA, HA, HA–NSc NPs, and celecoxib; n = 5 for each group) to ensure uniform baseline values for pain threshold and weight bearing. On Day 1, OA was induced by i.a. injection of 50 μL of MIA (30 mg mL^{-1}, dissolved in saline) into the right hind limb, excluding the Sham group. Three days after the MIA injection, 100 μL of saline, HA (10 mg kg^{-1}), HA–NSc (10 mg kg^{-1}) was directly injected into the joint once a week (Day 3, Day 10, and Day 17). Celecoxib (30 mg kg^{-1}), a commercial OA drug, was administered orally at 1 mL per day starting from Day 3. Body weight was measured once a week, and nociceptive threshold and weight bearing capacity were assessed twice a week. Monitoring was conducted for a total of 3 weeks, and the animals were sacrificed on Day 21. Nociceptive threshold and weight bearing measurements[51] were performed as follows:

2.14.1. Measurement of nociceptive threshold (mechanical withdrawal responses). The pain threshold was measured using a dynamic plantar aesthesiometer (Ugo Basile, 37400, Comerio, Italy), which gradually increases the force applied to

the animal's paw over time. The measurements were carried out in an acrylic box with a lower section made of a wire mesh bench. A metal filament was installed in the center of the right hind paw of the rat, and the experiment was conducted after acclimatizing the rat to the acrylic box for 5 min. A force ranging from 0 to 50 g was gradually applied for 10 s, and the measurement recorded the paw withdrawal latency (s) (PWL) and paw withdrawal threshold (g) (PWT) representing the rat's paw withdrawal behavior.

2.14.2. Measurement of weight bearing performance. This experiment measured the change in weight bearing between a normal hindlimb (left) and an OA hindlimb (right) due to knee pain in the OA hindlimb. The weight of each hind paw was measured using an incapacitance tester (Model 600, IITC, USA). Before measurement, rats were allowed to acclimate to the acrylic box for 5 min. Once accurately positioned in the holder within the acrylic box, the machine was operated. The measurement lasted 5 s, and after two measurements were taken, the average value was used as the weight bearing (g) value for each foot. The weight bearing results were analyzed by converting them to a weight bearing ratio.

$$\text{Weight bearing ratio} = \frac{\text{weight of right hind limb}}{(\text{weight of right hind limb}) + (\text{weight of left hind limb})} \times 100$$

2.15. Histological assay

After the conclusion of monitoring on Day 21, knee joint tissues were obtained through sacrifice. These knee joint tissues were fixed in formalin, deoxidized, and paraffin blocks were produced. The sections obtained from paraffin blocks were stained of Safranin O or subjected to immunohistochemical staining using the following antibodies: MMP-1 antibody (Abcam, ab137332, 1 : 250), MMP-13 antibody (Abcam, ab39012, 1 : 300), and IL-1β antibody (NOVIS, NB600-633, 1 : 500) (n = 3). Safranin O-stained tissues were evaluated using the OARSI[52] (Osteoarthritis Research Society International) and Mankin scoring[53] according to the evaluation indices. Additionally, tissues stained with MMP-1, MMP-13, IL-1β antibodies were examined through microscopy, and the positive area was analyzed and quantified.

2.16. Statistical analysis

All statistical analyses were conducted using GraphPad Prism 7 software. The results of the Griess assay and DAF-2 assay were analyzed using Student's t-test. The data of *in vitro* nitrite levels and cytokine levels were presented as mean ± SD and analyzed using one-way ANOVA. The results of *in vivo* PWL, PWT, and weight bearing were presented as mean ± SEM. Data for OARSI score, total Mankin score, and MMP-1, MMP-13, IL-1β positive areas were presented as mean ± SD. All *in vivo* data were analyzed using one-way ANOVA.

3. Results and discussion

3.1. Synthesis of HA–NSc conjugate

The NO scavenger NSc, equipped with an aminobutly group for polymer conjugation, was successfully synthesized through a three-step process (Fig. 1A). The synthesis began with a reaction between 4-chloro-3-nitrotoluene and *N*-Boc-1,4-butanediamine, followed by the hydrogenation of the nitro group to an amine group using H_2 in the presence of Pd/C. Then, the boc group was deprotected under acidic conditions to yield NSc. Each step of the synthesis was confirmed by ^{1}H NMR and ESI-MS (Fig. S1–3†). Finally, the HA–NSc conjugate was synthesized by conjugation of the synthesized NSc to the HA backbone *via* carbodiimide coupling agent EDC/HOBt (Fig. 1B).

The successful synthesis of HA–NSc conjugate was verified through ^{1}H NMR (Fig. 2A and S4†), UV-Vis spectra (Fig. 2B), and GPC (Fig. S5†). The ^{1}H spectrum of the HA–NSc conjugate clearly demonstrated the conjugation of NSc to HA, showing the presence of specific aromatic peaks of NSc. The distinct absorbance peaks of NSc at 290 nm and 378 nm were slightly shift to 288 nm and 374 nm when NSc was conjugated to HA in the HA–NSc conjugate. The GPC chromatogram showed a monomodal distribution with a peak shifted toward higher molecular weight, corroborating the successful synthesis of the purified HA–NSc conjugate. Moreover, the DS of NSc in the HA–NSc conjugate was calculated by comparing the peak integrals of the *N*-acetyl (–$NHCOCH_3$) peak of HA and the methyl (–CH_3) peak of NSc, revealing approximately 107.5 NSc molecules per one HA polymer chain. The molecular weights derived from ^{1}H NMR and GPC, along with the polydispersity index (PDI) values, were summarized in Table 1.

3.2. Characterization of self-assembled HA–NSc NPs

Importantly, the amphiphilic nature of the HA–NSc conjugate facilitated the formation of self-assembled spherical nanoparticles in an aqueous condition with an average size of 406.9 ± 9.4 nm as determined by DLS (Fig. 2C), while HA alone did not form any nanoparticles (Fig. S6†). In OA pathology, NO is known to be overexpressed in the joints, and high concentrations of NO can lead to the oxidative degradation of HA which affects its therapeutic efficiency.[54] Furthermore, the degradation or removal of HA in response to NO might compromise the lubricant properties of HA.[12,54] The introduction of HA–NSc NPs offers a promising solution to this issue, as these NPs can scavenge NO, thereby reducing its concentration and preserving the integrity of HA polymer. To investigate integrity of the polymer under NO conditions, GPC traces of the HA and HA–NSc conjugate were recorded before and after incubation with NO (Fig. S7†). In the absence of NO, HA showed a single peak with a retention of 13.6 min. However, after incubation with 100 μM (ref. 22 and 23) concentration, a level typical in OA joints, an additional new peak was observed with a retention time of 18.2 min, indicating the fragmentation of HA polymer chain. Remarkably, HA–NSc maintained a single peak with a retention time of 13.4 min even after exposed to high NO concentrations. These results clearly indi-

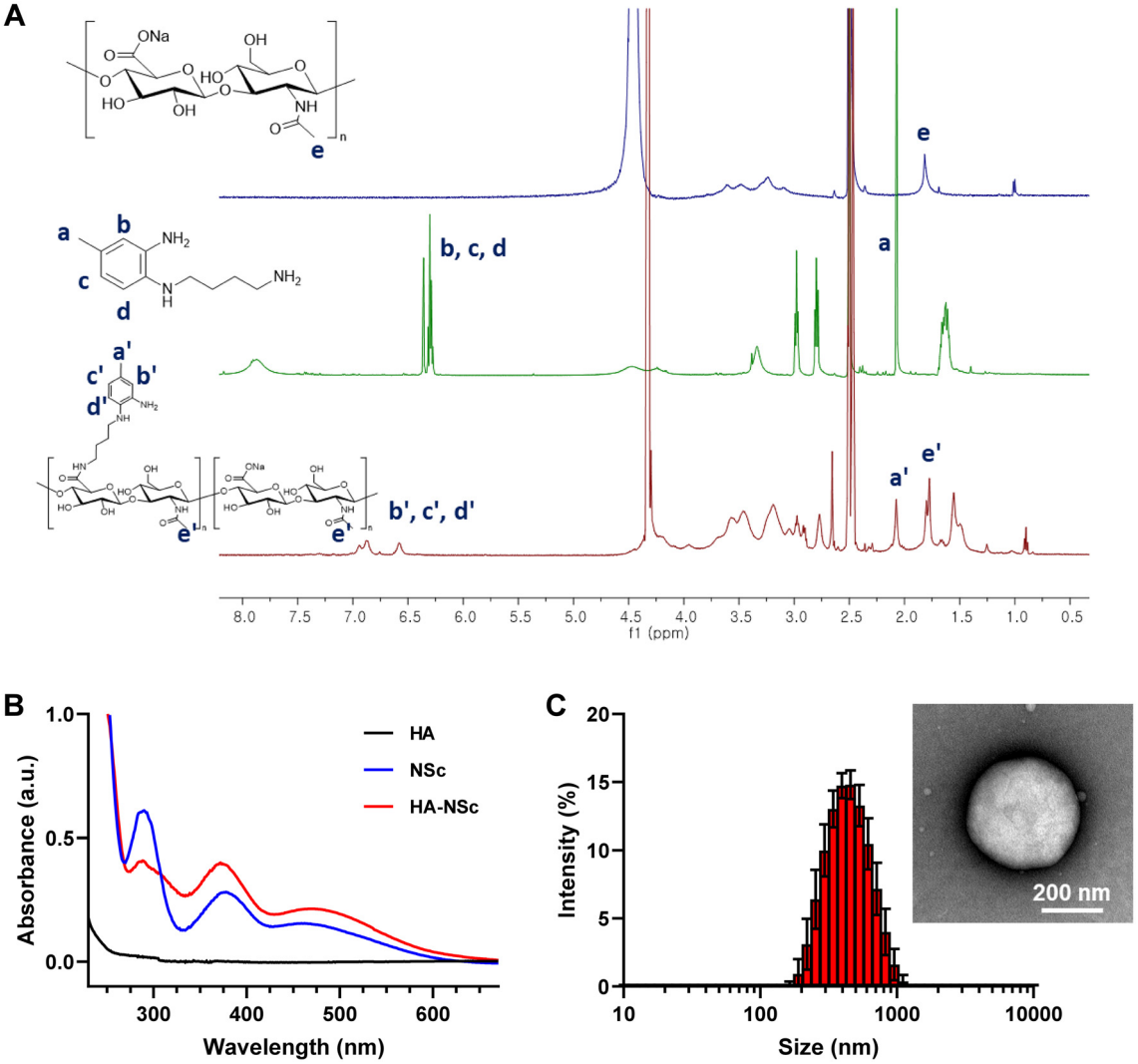

Fig. 2 Synthesis of HA–NSc conjugate and self-assembled nanoparticles. (A) ^{1}H NMR spectra and (B) UV-Vis spectra of HA, NSc, and HA–NSc conjugate. (C) Size distribution and TEM image (inserted picture) of self-assembled HA–NSc NPs (scale bar = 200 nm).

Table 1 Properties of HA and HA–NSc conjugate

Polymer	M_n, NMR (kDa)	M_n, GPC (kDa)	M_w, GPC (kDa)	M_w/M_n, GPC
HA	100	136.415	182.66	1.339
HA–NSc	120.779	156.223	245.427	1.571

cate that the NO-scavenging ability of HA–NSc can prevent its chain fragmentation even under high NO conditions, which is one of the important properties required for its therapeutic potential.

Subsequently, the stability of the HA–NSc NPs under NO condition was analyzed using DLS and TEM (Fig. 3A and B). After exposure to NO, the hydrodynamic size of the HA–NSc NPs slightly decreased to 271.2 ± 9.1 nm, but their morphology remained spherical. The reduction in size of these nanoparticles may be due to the formation of a dense hydrophobic benzotriazole core as a result of the reaction of NO with NSc. Despite exposure to NO, these HA–NSc NPs exhibited high stability without any polymer chain degradation, indicating their suitability for use in NO-rich pathological environments such as OA.

3.3. NO scavenging ability of HA–NSc NPs

After confirming the stability of HA–NSc NPs, their NO scavenging capability was studied in detail. In general, *o*-PD and its derivatives are known to react with NO in the presence of O_2 to form a benzotriazole derivatives.[38,39] First, the ability of NSc and HA–NSc conjugate to scavenge NO and the formation of benzotriazole was determined using ^{1}H NMR spectroscopy and UV-Vis spectroscopy (Fig. S8†).[36,37] Upon reaction with NO, both NSc and the HA–NSc conjugate showed distinct spectral changes in the ^{1}H NMR, in which the peak corresponding to the primary amine of the *o*-PD moiety disappeared and the characteristics aromatic peaks shifted. Additionally, the absor-

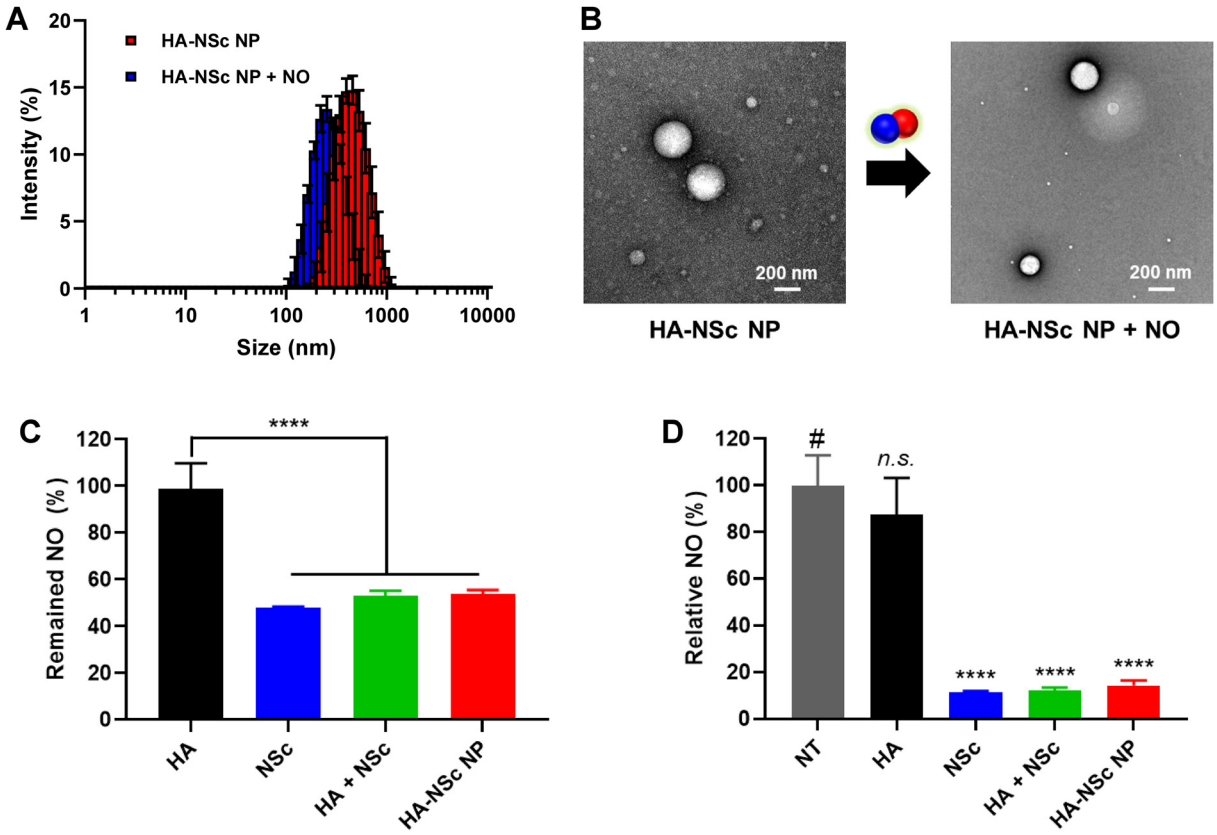

Fig. 3 Characterization of HA–Nsc NPs. The hydrodynamic size distribution (A) and morphology change (B) of HA–NSc NPs before and after NO incubation were confirmed by DLS and TEM (scale bar = 200 nm). NO scavenging properties of HA–NSc NPs were evaluated by Griess assay (C) and DAF-2 assay (D) (n = 5, mean ± SD, ****p < 0.0001).

bance at the wavelength of 280–300 nm, which corresponds to benzotriazole derivatives, exhibited a noticeable increase for both the samples after reaction with NO.

Having established the capability of NSc and HA–NSc to react with NO, we aimed to quantify their NO scavenging efficiency. The Griess assay, a standard method for quantifying nitrite concentration, was employed to assess the NO scavenging efficiency of, NSc, HA–NSc NPs, HA, and HA + NSc physical mixture. The typical NO donor, PyNO was used as the source of NO.[36] As the sample concentration increased, the NO scavenging ability generally enhanced, except in the HA group (Fig. S9†). In particular, HA–NSc NPs demonstrated similar NO scavenging efficiency to NSc alone while HA by itself showed no efficacy in scavenging NO (Fig. 3C). To further confirm these results, an additional NO scavenging assay, the DAF-2 assay, was performed (Fig. 3D). DAF-2 is a specific fluorescent probe for NO. It reacts with NO in the presence of O_2 to yield the highly fluorescence DAF-2 triazole (DAF-2T). While HA showed no NO scavenging capacity, the group containing NSc effectively eliminated NO. Taken together, these experiments revealed that the NO scavenging efficiency of NSc remained robust even when conjugated to the HA backbone. Thus, HA–NSc NPs were confirmed to be effective NO scavengers.

3.4. *In vitro* cytotoxicity analysis and anti-inflammatory effects of HA–NSc NPs

The cytotoxicity of NSc and HA–NSc conjugate was evaluated using MTT assay. For this purpose, RAW 264.7 cell, a murine macrophage cell line known for their ability to produce high levels of NO and pro-inflammatory cytokines upon lipopolysaccharide (LPS) stimulation,[55,56] was utilized. As depicted in Fig. 4A and B, HA alone exhibited no toxicity. In contrast, samples with NSc demonstrated significant cytotoxicity against RAW 264.7 cells, both in the presence and absence of LPS. Notably, the HA–NSc conjugate exhibited less cytotoxicity than NSc or physical mixture of HA + Nsc, suggesting that chemical conjugation of NSc to the HA backbone significantly reduced the toxicity of NSc. The IC_{50} value of the HA–NSc was 3-fold higher than that of NSc or the HA + NSc mixture (Fig. S9†). These results suggest that the HA–NSc conjugate is a more suitable candidate for bioapplications compared to NSc alone or a mixture of HA and NSc.

To further ascertain the NO scavenging ability of HA–NSc NPs, a Griess assay was conducted in LPS-stimulated RAW 264.7 cell model (Fig. 4C). As expected, HA exhibited negligible NO scavenging capability. In contrast, groups with NSc (NSc,

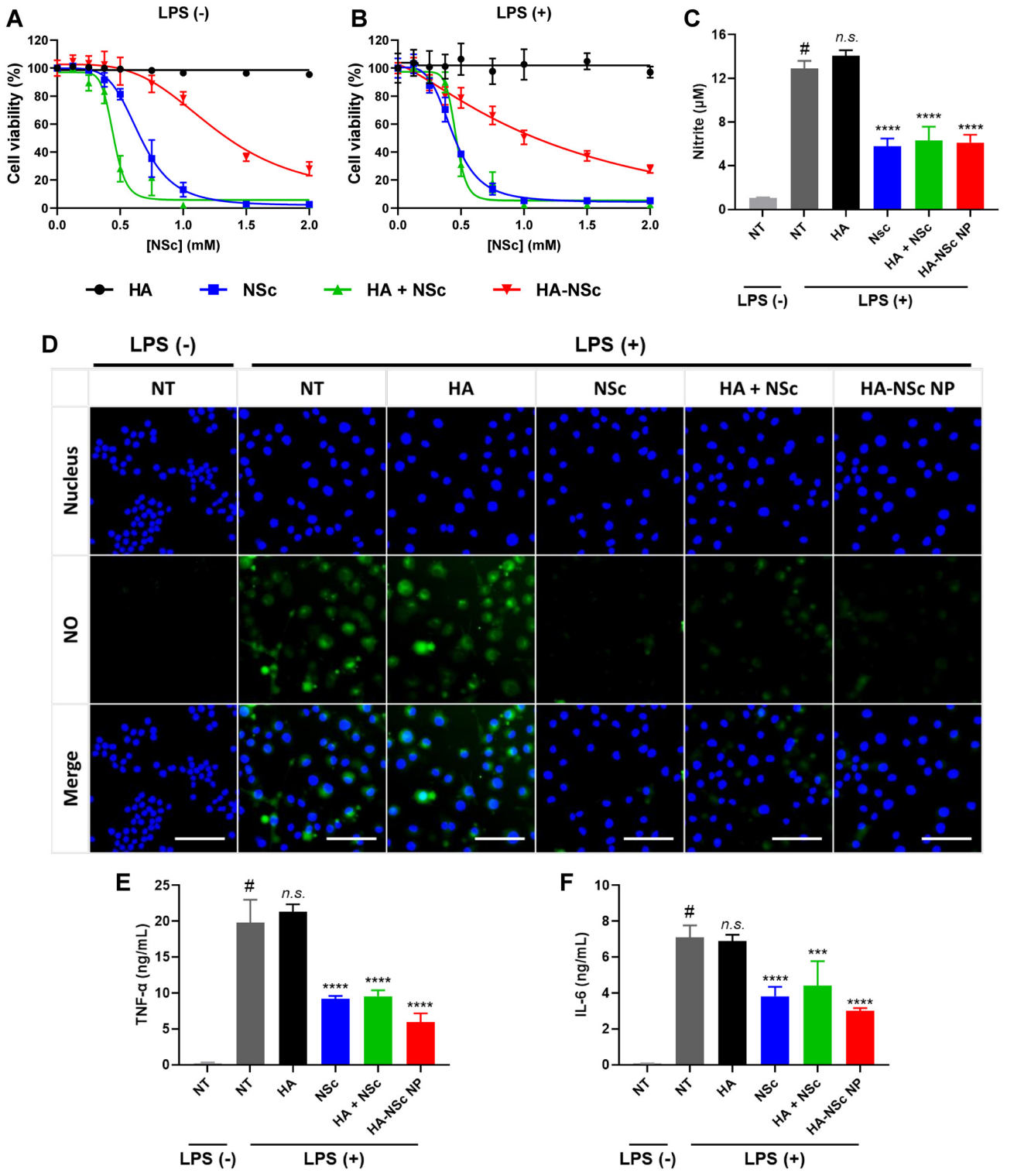

Fig. 4 Anti-inflammatory effects of HA–NSc NPs in LPS-stimulated RAW 264.7 cells. Cell cytotoxicity of HA, NSc, HA + NSc, and HA–NSc NPs against (A) LPS (–) and (B) LPS (+) RAW 264.7 cells (n = 5, mean ± SD). (C) *In vitro* NO scavenging ability of HA–NSc NPs evaluated by Griess assay (n = 4, mean ± SD, ****p < 0.0001). (D) Fluorescence images of intracellular NO levels of LPS (–) and LPS (+) RAW 264.7 cells after treatment of various samples. NO and nucleus were presented by DAF-FM DA (green, 5 μM) and Hoechst 33342 (blue, 10 μM) (scale bare = 50 μm). Quantification of pro-inflammatory cytokine (E) TNF-α and (F) IL-6 after treatment of various samples (n = 4, mean ± SD, ***p < 0.001, ****p < 0.0001).

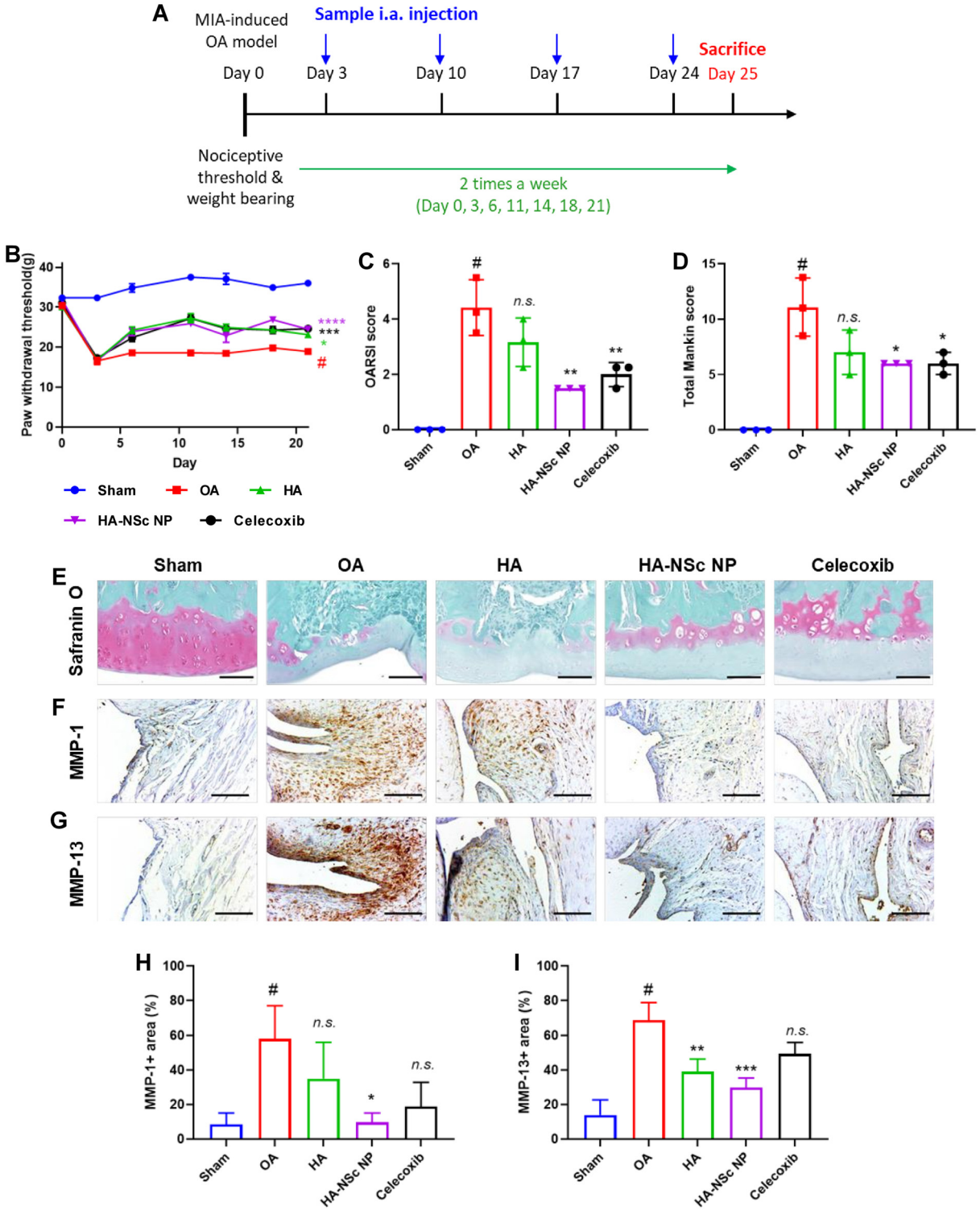

Fig. 5 *In vivo* therapeutic effects of HA–NSc NPs in OA treatment. (A) Experimental design of therapeutic effects of HA–NSc NPs in MIA-induced OA rat model. The 50 μL of MIA (30 mg mL^{-1}) was administered i.a. to induce OA model at Day 0. Saline, HA (10 mg kg^{-1}), and HA–NSc NPs (10 mg kg^{-1}) were injected i.a. once a week, and celecoxib (30 mg kg^{-1}) were orally administered every day. (B) Paw withdrawal responses to mechanical measurements during 21 days (n = 5, mean ± SEM, *p < 0.05, **p < 0.01, ***p < 0.001). Analysis of (C) OARSI score and (D) total Mankin score (n = 3, mean ± SD, *p < 0.05, **p < 0.01) (E) Safranin O staining and immunohistochemical staining of (F) MMP-1 and (G) MMP-13 of rat knee joint after monitoring (scale bar = 100 μm). Quantitative analysis of (H) MMP-1 and (I) MMP-13 positive area of rat knee joint (n = 3, mean ± SD, *p < 0.05).

HA–NSc NP, and HA + NSc mixture) demonstrated effective NO scavenging activities. Remarkably, there was no significant difference in the residual NO levels between the NSc and HA–NSc treatment groups, again indicating that the NO scavenging activity of NSc remains effective even when conjugated to HA.

To visualize the remained intracellular NO levels, the NO-specific cell-permeable fluorescent probe DAF-FM DA was employed (Fig. 4D). Upon LPS stimulation, RAW 264.7 cells exhibited an increase in intracellular NO levels, which significantly enhance the endogenous fluorescence intensity of DAF-FM DA. When the activated RAW 264.7 cells were treated with NSc, HA–NSc NP or HA + NSc mixture, a substantial reduction in fluorescence intensity was observed, whereas the fluorescence was not reduced for the HA-treated group. This further reinforces that HA does not influence the reduction of NO levels, only the NSc can effectively scavenge NO whether it is simply mixed with or chemically conjugated to HA.

Several reports suggest that elevated NO levels are associated with the production of pro-inflammatory cytokines, such as TNF-α, IL-6, and IL-1β.[55,56] These cytokine levels were quantified in LPS-stimulated macrophages following treatment with the samples (Fig. 4E and F). When RAW 264.7 cells were stimulated with LPS, the levels of pro-inflammatory cytokines (TNF-α, IL-6) were significantly increased. The treatment of activated cells with HA–NSc NPs having NO scavenging capabilities led to a significant reduction in these levels of pro-inflammatory cytokines, while HA treatment alone had no such effect. These results indicate the potential of HA–NSc NPs for the anti-inflammatory treatment by scavenging NO. Overall, the HA–NSc NPs demonstrated an excellent NO-scavenging ability, low cytotoxicity and ability to reduce the pro-inflammatory cytokines in *in vitro* conditions, suggesting as a promising candidate for anti-inflammatory *in vivo* applications.

3.5. Therapeutic effects of HA–NSc NPs in OA animal model

Finally, we evaluated the therapeutic effects of HA–NSc NPs in a monosodium iodoacetate (MIA)-induced rat as an OA animal model. Intra-articular (i.a.) injection of MIA triggers the activation of MMPs, leading to cartilage degradation and OA development.[57–59] The therapeutic experiment followed the schedule shown in Fig. 5A. Three days post-OA induction in the right hindlimb *via* MIA injection, samples (saline, HA, and HA–NSc NPs) were administered i.a. once a week. Celecoxib, a COX-2 inhibitor, was employed as a positive control and was given by mouth once a day during the observation period.

Pain threshold was assessed using an Electronic Von Frey system, with outcomes expressed as the paw withdrawal threshold (PWT) and paw withdrawal latency (PWL). The weight-bearing activities were measured using an incapacitance tester, allowing separate hind limb weigh bearing measurements, expressed as a weight bearing ratio. While there was no improvement in weight-bearing measurements across all groups, the HA–NSc NPs, HA, and celecoxib treatment groups demonstrated significant improvement in paw withdrawal behavior compared to the sham group (Fig. 5B and S10†). Furthermore, no decrease in body weight was observed, indicating that there was no critical toxicity of HA–NSc NPs (Fig. S11†). These results suggest that HA, acting as a lubricant, is somewhat effective in alleviating pain, and this lubricant effect is maintained even when the NSc is conjugated to HA (HA–NSc NPs).

Post-monitoring, knee joints were isolated, and Safranin O staining was performed (Fig. 5E). Subsequently, cartilage degradation was evaluated using the OARSI and Mankin scores (Fig. 5C and D).[52,53] These scores provide numerical standards for the degree of joint destruction and severity of OA. While the HA treatment group showed no effect in preventing cartilage destruction in the Safranin O staining and scorings, HA–NSc NPs significantly reduced cartilage damage and preserved the intact tidemark. Additionally, immunohistochemical staining for MMP-1 (Fig. 5F and H) and MMP-13 (Fig. 5G and I) were conducted on isolated knee joints, and the quantification of their expression area were analyzed. Overexpressed MMPs (MMP-1, 3, 13, *etc*.) are directly linked to cartilage destruction and are associated with abnormal NO levels in OA.[28,35] The expression of MMP-1 and MMP-13 was significantly decreased following i.a. injection of HA–NSc NPs, suggesting that a strategy aimed at reducing NO levels in the joints can prevent overexpression of MMPs. Furthermore, immunohistochemical staining of IL-1β and its quantification were conducted (Fig. S12†). Although expression of IL-1β was slightly reduced in the HA-NSc NPs-treated group compared with the OA disease group, it did not reach statistical significance.

Taken together, the HA–NSc NPs that combine the dual functionality lubricating ability of HA and NO scavenging ability of NSc offer a promising strategy to prevent cartilage destruction and severe inflammation. As a lubricant, the HA–NSc NPs alleviate pain, and by scavenging NO, HA–NSc NPs help prevent joint destruction and overexpression of MMP-1 and MMP-13. These results from this study suggest HA–NSc NPs as a promising anti-inflammatory agent and provide a potent therapeutic avenue for the effective management of OA.

4. Conclusions

In this study, we have successfully synthesized self-assembled HA–NSc NP that exhibits dual functionality, as a lubricant and anti-inflammatory agent, using the HA–NSc conjugate. This novel conjugate was synthesized through facile conjugation of the NSc, a NO-scavenging *o*-PD derivative, to the HA backbone. The HA–NSc NPs maintained its structural stability even under high NO conditions because of the NO-scavenging capacity of the NSc moieties, thereby preserving the lubricant properties of HA. This NO-scavenging ability of the HA–NSc NPs also effectively reduced the levels of pro-inflammatory cytokines, alleviated pain, and mitigated joint damage in an OA model. Remarkably, our findings underscore that reducing the concentration of NO, a pivotal inflammatory factor in OA, not only exerts potent anti-inflammatory effects but also prevents joint deterioration by reducing the expression of MMP-1 and MMP-13. While comprehensive investigations are still required

to fully harness the potential of HA–NSc NPs, the results indicate their superior efficacy compared to both HA alone and the therapeutic drug, celecoxib. As mentioned earlier, this enhanced effectiveness can be attributed to their ability to protect HA from degradation through NO scavenging and to prolong intra-articular retention time by forming nanoparticles. In summary, this study highlights the potential of HA–NSc NPs as a promising therapeutic agent for the treatment OA, showing a novel approach that combines lubrication with targeted anti-inflammatory action.

Author contributions

This study was designed by Y. N. and W. J. K., and performed experiments and analyzed the data by S. S., G. S., B. Y. K., and J. B. Y. The overall research was supervised by W. J. K. The manuscript was written by Y. N. and W. J. K.

Conflicts of interest

W. J. K. is the CEO of the OmniaMed, but declares no conflict of interest of this paper.

Acknowledgements

This study was supported by the National Research Foundation of Korea (NRF) Grant (NRF-2022R1A3B1077354, RS-2023-00302525, RS-2023-00260454) and the Creative Materials Discovery Program (NRF-2018M3D1A1058813) funded by the Korea government (Ministry of Science and ICT).

References

1 J. Martel-Pelletier, A. J. Barr, F. M. Cicuttini, P. G. Conaghan, C. Cooper, M. B. Goldring, S. R. Goldring, G. Jones, A. J. Teichtahl and J.-P. Pelletier, *Nat. Rev. Dis. Primers*, 2016, **2**, 16072.
2 R. F. Loeser, S. R. Goldring, C. R. Scanzello and M. B. Goldring, *Arthritis Rheum.*, 2012, **64**, 1697–1707.
3 M. Y. Ansari, N. Ahmad and T. M. Haqqi, *Biomed. Pharmacother.*, 2020, **129**, 110452.
4 Q. Yao, X. Wu, C. Tao, W. Gong, M. Chen, M. Qu, Y. Zhong, T. He, S. Chen and G. Xiao, *Signal Transduction Targeted Ther.*, 2023, **8**, 56.
5 H. A. Wieland, M. Michaelis, B. J. Kirschbaum and K. A. Rudolphi, *Nat. Rev. Drug Discovery*, 2005, **4**, 331–344.
6 W. Wang, Y. Niu and Q. Jia, *Front. Physiol.*, 2022, **13**, 1011407.
7 J. Wen, H. Li, H. Dai, S. Hua, X. Long, H. Li, S. Ivanovski and C. Xu, *Mater. Today Bio*, 2023, **19**, 100597.
8 G. B. D. O. Collaborators, *Lancet Rheumatol.*, 2023, **5**, e508–e522.
9 A. Latourte, M. Kloppenburg and P. Richette, *Nat. Rev. Rheumatol.*, 2020, **16**, 673–688.
10 S. L. Kolasinski, T. Neogi, M. C. Hochberg, C. Oatis, G. Guyatt, J. Block, L. Callahan, C. Copenhaver, C. Dodge, D. Felson, K. Gellar, W. F. Harvey, G. Hawker, E. Herzig, C. K. Kwoh, A. E. Nelson, J. Samuels, C. Scanzello, D. White, B. Wise, R. D. Altman, D. DiRenzo, J. Fontanarosa, G. Giradi, M. Ishimori, D. Misra, A. A. Shah, A. K. Shmagel, L. M. Thoma, M. Turgunbaev, A. S. Turner and J. Reston, *Arthritis Rheumatol.*, 2020, **72**, 220–233.
11 H. Lu, J. Wei, K. Liu, Z. Li, T. Xu, D. Yang, Q. Gao, H. Xiang, G. Li and Y. Chen, *ACS Nano*, 2023, **17**, 6131–6146.
12 W. Liu, M. Ma, Z. Lei, Z. Xiong, T. Tao, P. Lei, Y. Hu, X. Jiang and J. Xiao, *Mater. Des.*, 2022, **217**, 110579.
13 T. Neogi, S. Li, C. Peloquin, D. Misra and Y. Zhang, *Ann. Rheum. Dis.*, 2018, **77**, 92–97.
14 A. Lanas, J. Tornero and J. L. Zamorano, *Ann. Rheum. Dis.*, 2010, **69**, 1453–1458.
15 F. E. Silverstein, G. Faich, J. L. Goldstein, L. S. Simon, T. Pincus, A. Whelton, R. Makuch, G. Eisen, N. M. Agrawal, W. F. Stenson, A. M. Burr, W. W. Zhao, J. D. Kent, J. B. Lefkowith, K. M. Verburg and G. S. Geis, *J. Am. Med. Assoc.*, 2000, **284**, 1247–1255.
16 S. Brown, S. Kumar and B. Sharma, *Acta Biomater.*, 2019, **93**, 239–257.
17 C. Wainwright, J. C. Theis, N. Garneti and M. Melloh, *J. Bone Jt. Surg., Br. Vol.*, 2011, **93-B**, 1411–1415.
18 S. M. Heo, I. Harris, J. Naylor and A. M. Lewin, *BMC Musculoskeletal Disord.*, 2020, **21**, 602.
19 A. W. Carpenter and M. H. Schoenfisch, *Chem. Soc. Rev.*, 2012, **41**, 3742–3752.
20 Z. Wang, A. Jin, Z. Yang and W. Huang, *ACS Nano*, 2023, **17**, 8935–8965.
21 A. Karan, M. A. Karan, P. Vural, N. Erten, C. Tascioglu, C. Aksoy, M. Canbaz and A. Oncel, *Clin. Rheumatol.*, 2003, **22**, 397–399.
22 S. Karatay, A. Kiziltunc, K. Yildirim, R. C. Karanfil and K. Senel, *Clin. Rheumatol.*, 2005, **24**, 497–501.
23 P. Jin, G. Xu, X. Chen, S. C. Li, L. Cheng, P. Sui, J. Ye, X. Yang, S. Xi, F. Yu and T. Jiang, *J. Mater. Chem. B*, 2023, **11**, 2145–2156.
24 P. S. Grabowski, A. J. England, R. Dykhuizen, M. Copland, N. Benjamin, D. M. Reid and S. H. Ralston, *Arthritis Rheum.*, 1996, **39**, 643–647.
25 G. Kolios, V. Valatas and S. G. Ward, *Immunology*, 2004, **113**, 427–437.
26 T. Kim, Y. Nah, J. Kim, S. Lee and W. J. Kim, *Acc. Chem. Res.*, 2022, **55**, 2384–2396.
27 B. Fermor, J. B. Weinberg, D. S. Pisetsky, M. A. Misukonis, A. J. Banes and F. Guilak, *J. Orthop. Res.*, 2001, **19**, 729–737.
28 H. Jiang, P. Ji, X. Shang and Y. Zhou, *Molecules*, 2023, **28**, 1683–1905.
29 S. B. Abramson, *Osteoarthr. Cartil.*, 2008, **16**, S15–S20.

30 S. Hashimoto, K. Takahashi, D. Amiel, R. D. Coutts and M. Lotz, *Arthritis Rheum.*, 1998, **41**, 1266–1274.
31 R. J. Van'T Hof and S. H. Ralston, *Immunology*, 2001, **103**, 255–261.
32 J. A. Roman-Blas and S. A. Jimenez, *Osteoarthr. Cartil.*, 2006, **14**, 839–848.
33 R. M. Clancy, P. F. Gomez and S. B. Abramson, *Osteoarthr. Cartil.*, 2004, **12**, 552–558.
34 M. C. Choi, J. Jo, J. Park, H. K. Kang and Y. Park, *Cells*, 2019, **8**, 734.
35 N. Ahmad, M. Y. Ansari and T. M. Haqqi, *J. Cell Physiol.*, 2020, **235**, 6366–6376.
36 J. Yeo, Y. M. Lee, J. Lee, D. Park, K. Kim, J. Kim, J. Park and W. J. Kim, *Nano Lett.*, 2019, **19**, 6716–6724.
37 T. Kim, J. Suh and W. J. Kim, *Adv. Mater.*, 2021, **33**, e2008793.
38 Y. M. Lee, S. Lee and W. J. Kim, *Biomater. Sci.*, 2023, **11**, 2395–2404.
39 J. Park, S. Pramanick, D. Park, J. Yeo, J. Lee, H. Lee and W. J. Kim, *Adv. Mater.*, 2017, **29**, 1702859.
40 J. Kim, L. F. Sestito, S. Im, W. J. Kim and S. N. Thomas, *Adv. Funct. Mater.*, 2020, **30**, 1908788.
41 Z. Fan, J. Li, J. Liu, H. Jiao and B. Liu, *ACS Appl. Mater. Interfaces*, 2018, **10**, 23595–23604.
42 Q. Hu, F. Zhang, Y. Wei, J. Liu, Y. Nie, J. Xie, L. Yang, R. Luo, B. Shen and Y. Wang, *Biomacromolecules*, 2023, **24**, 3532–3544.
43 K. Ren, H. Wan, H. J. Kaper and P. K. Sharma, *J. Colloid Interface Sci.*, 2022, **619**, 207–218.
44 Y. S. Kim and F. Guilak, *Int. J. Mol. Sci.*, 2022, **23**, 8662.
45 A. Homma, H. Sato, A. Okamachi, T. Emura, T. Ishizawa, T. Kato, T. Matsuura, S. Sato, T. Tamura, Y. Higuchi, T. Watanabe, H. Kitamura, K. Asanuma, T. Yamazaki, M. Ikemi, H. Kitagawa, T. Morikawa, H. Ikeya, K. Maeda, K. Takahashi, K. Nohmi, N. Izutani, M. Kanda and R. Suzuki, *Bioorg. Med. Chem.*, 2009, **17**, 4647–4656.
46 Q. Jiang and S. Zhang, *Small*, 2023, **19**, 2206929.
47 C. H. Evans, V. B. Kraus and L. A. Setton, *Nat. Rev. Rheumatol.*, 2014, **10**, 11–22.
48 T. K. Mwangi, I. M. Berke, E. H. Nieves, R. D. Bell, S. B. Adams and L. A. Setton, *J. Controlled Release*, 2018, **283**, 76–83.
49 R. Ferrero, F. Rodríguez-Pascual, M. T. Miras-Portugal and M. Torres, *Br. J. Pharmacol.*, 1999, **127**, 779–787.
50 M. N. Möller, N. Rios, M. Trujillo, R. Radi, A. Denicola and B. Alvarez, *J. Biol. Chem.*, 2019, **294**, 14776–14802.
51 J. R. Deuis, L. S. Dvorakova and I. Vetter, *Front. Mol. Neurosci.*, 2017, **10**, 284.
52 S. S. Glasson, M. G. Chambers, W. B. Van Den Berg and C. B. Little, *Osteoarthr. Cartil.*, 2010, **18**, S17–S23.
53 H. J. Mankin, H. Dorfman, L. Lippiello and A. Zarins, *J. Bone Jt. Surg.*, 1971, **53**, 523–537.
54 A. M. Alsharabasy, S. Glynn, P. Farràs and A. Pandit, *Biomacromolecules*, 2022, **23**, 3621–3647.
55 Y. Yan, A. Lu, Y. Dou, Z. Zhang, X. Y. Wang, L. Zhai, L. Y. Ai, M. Z. Du, L. X. Jiang, Y. J. Zhu, Y. J. Shi, X. Y. Liu, D. Jiang and J. C. Wang, *Adv. Sci.*, 2023, **10**, e2207490.
56 J. K. Kang, Y. C. Chung and C. G. Hyun, *Molecules*, 2021, **26**, 5351.
57 R. X. Zhang, K. Ren and R. Dubner, *Osteoarthr. Cartil.*, 2013, **21**, 1308–1315.
58 E. L. Kuyinu, G. Narayanan, L. S. Nair and C. T. Laurencin, *J. Orthop. Surg. Res.*, 2016, **11**, 19.
59 P. R. Chiu, Y. C. Hu, T. C. Huang, B. S. Hsieh, J. P. Yeh, H. L. Cheng, L. W. Huang and K. L. Chang, *Int. J. Mol. Sci.*, 2017, **18**, 38.